Dynamics of Atmospheres and Oceans 66 (2014) 58–76

Contents lists available at ScienceDirect

Dynamics of Atmospheres and Oceans

journal homepage: www.elsevier.com/locate/dynatmoce

Characterizing turbulent overturns in CTD-data

Hans van Haren[a,*], Louis Gostiaux[b]

[a] Royal Netherlands Institute for Sea Research (NIOZ), P.O. Box 59, 1790 AB Den Burg, The Netherlands
[b] Laboratoire de Mécanique des Fluides et d'Acoustique, UMR CNRS 5509, École Centrale de Lyon, Université de Lyon, 36 avenue Guy de Collongue, 69134 Écully Cedex, France

A R T I C L E   I N F O

Article history:
Received 1 October 2013
Received in revised form 3 February 2014
Accepted 4 February 2014
Available online 15 February 2014

Keywords:
Overturn character
Rankine vortex model
Vertical profile (CTD) observations

A B S T R A C T

We are concerned with the shape of overturns due to irreversible effects of turbulent mixing through internal wave breaking in the ocean. Vertical (z) overturn displacements (d) are computed from ship-borne SeaBird-911 CTD-data using the well-established method of reordering unstable portions in vertical density profiles. When displayed as a function of z, the displacements $d(z)$ reveal a characteristic zigzag shape. Here, we primarily investigate the particular slope (z/d) of this zigzag signature after assigning the displacements to the end-point depths. Using model-overturns we show that this slope equals ½ for a solid-body-rotation, while a more sophisticated Rankine-vortex overturn-model, here employed in the vertical, has slopes slightly >½ in the interior and >1 along the sides. In the case of a near-homogeneous layer, displacement-points fill a parallelogram with side-edges having a slope of 1. The models are used to interpret overturn shapes in NE-Atlantic-Ocean-data from moderately deep, turbulent waters above Rockall Bank (off Ireland) and from deep, weakly stratified waters above Mount Josephine (off Portugal). These are compared with salinity-compensated intrusion data in Mediterranean-outflow-waters in the Canary Basin. Dynamically, most overturns are found to resemble the half-turn Rankine-vortex model and very few a, small-only, solid-body-rotation. Additionally, the usefulness and uselessness of upcast-CTD-data are discussed for overturn characterization.

* Corresponding author. Tel.: +31 222 369300/369451.
E-mail address: hans.van.haren@nioz.nl (H. van Haren).

http://dx.doi.org/10.1016/j.dynatmoce.2014.02.001
0377-0265/

1. Introduction

The study of turbulent exchange is vital for living organisms in the ocean, as it constitutes a major means of transporting (fluxing) of nutrients into the photic zone. It is also important for the redistribution of materials in general, sediment in particular. One of the major contributors to the mechanical generation of turbulence in the ocean is the breaking of 'internal' waves (e.g., Shrira, 1981; Gregg, 1989). Such waves are supported by the ocean's stratification in density from surface to bottom. Depending on temperature and salinity variations, the vertical density stratification determines the buoyancy frequency N, the natural frequency of gravity oscillations of the shortest internal wave period (Groen, 1948; demonstrated with observations by, e.g., Cairns and Williams, 1976; van Haren, 2005). It can thus be used as a separator between freely propagating internal waves, for frequencies $\sigma < N$, and turbulent overturns, or more precisely overturning: active mixing, for $\sigma \geq N$.

Typical internal wave periods range from one day (10^5 s; at mid-latitudes) to one hour (10^4 s), in the deep ocean, and a few minutes (10^2 s), near the ocean surface (LeBlond and Mysak, 1978). Turbulence time scales range from 10^{-2} s (shortest dissipation scales) to 10^3 s (largest overturn scales) (Jiménez, 1997). In the spatial domain, internal-wave-generated turbulence scales vary from several tens of meters (the internal wave height and the buoyancy scale) to a few millimeters (the dissipation scale). In the open-ocean interior, internal waves are ubiquitous causing permanent motion (e.g., Marmorino et al., 1987) but their turbulence generation is relatively weak there (e.g., Gregg, 1989; Polzin et al., 1996). It seems that most turbulence is generated where internal waves 'beach', at underwater topography.

There are several means to observe internal waves and several ways to observe turbulence in the ocean. However, few means exist that partially cover both phenomena so that studies on the effect of internal wave-induced mixing are limited. One of the reasons for this limited observational evidence of internal wave mixing is that density (variations) cannot be measured directly. One has to measure temperature T and salinity S (variations) as a function of pressure (depth). Of these two quantities, the measurement of salinity is most difficult, as it is done indirectly via conductivity, which itself is highly temperature dependent. This requires a combination of two sensors with different characteristics. It results in relatively large noise levels compared to the measurement of temperature. However, one could refrain from salinity measurements, most conveniently under the condition of a tight (linear, persistent with time) T–S relationship. Such a relationship holds in surprisingly many ocean areas, although not in all and not always.

The most common instrument for observing turbulence is via tethered ('ship-borne') or free-falling microstructure profilers. They measure shear, and nowadays in most occasions also temperature, variance down to very small (10^{-2} m) near-dissipation vertical scales. The data are binned over larger vertical scales of typically 10 m and cast in spectra (e.g., Oakey, 1982). The comparison of these spectra with theoretical Nasmyth-, and Batchelor-, spectra provides estimates of turbulence parameters like dissipation rate and, indirectly following some assumptions, eddy diffusivity. The same data could also be used to estimate 'overturning displacements', introduced by Thorpe (1977) and their rms-value are now known as 'Thorpe scales'. After establishment of a relationship between Thorpe scales and Ozmidov scales of the largest overturning at a given buoyancy frequency by Dillon (1982) one arrives at turbulence parameter estimates, which agree reasonably in quite some cases, to within a factor of 2, with microstructure shear-probe data (Oakey, 1982; Ferron et al., 1998; Hosegood et al., 2005). However, overturning scales are seldom computed using microstructure profiler data. Notable exceptions are described by Ferron et al. (1998) and Stansfield et al. (2001), who found mean values of their turbulence dissipation rates from such scales to agree with those from shear-probe data to within 15%. Ferron et al. (1998) also compared overturn displacements from regular CTD-data in the same area, both computed for temperature only and for density (temperature and salinity) data. In general, all methods agreed to within a factor of two for mean values, except for density data when a strict data criterion of four times the standard error was applied. It was concluded that CTD-density data are, in general, too noisy and that better temperature-only data are used. This will be confirmed here. If one would use density profiles for overturn estimates, the expense will be reduced turbulence rates as such estimates are made under an extra condition of data 'de-spiking' (Gargett and Garner, 2008).

In the present paper, we propose a different approach and investigate the dynamical nature of overturns from their shape. To this purpose, we use SeaBird 911 CTD-data from various North-East-Atlantic sites. As turbulent mixing estimates rely on the theoretical fate of an overturn (and on the resulting transfer of kinetic into potential energy), the correct characterization of an overturn and of its dynamics is, in our view, the first step of an accurate mixing estimation. Here, with the aid of simple characteristic vortex models, it is found that the shape of displacements indicates the level of true overturns and the level of noise. The steepness of slope of the displacement-shape characterizes the dynamics of gravitational collapse. It can thus be used to establish the overturning time-scale and the inertial-buoyancy balance, or lack thereof. Technically, the difference between turbulence parameters using down- or upcast-data is shown to amount up to a factor of five. Nonetheless, upcast-CTD-data can be useful for discrimination between 'true' and 'false' turbulent overturns. Also, the difference between displacements using temperature-only and using density (temperature and salinity) is investigated. This is important for discriminating salinity-compensated inversions in the much less noisy temperature-only estimates.

Although we focus on the dynamical and technical physical aspects of overturns, we also aim to advocate the importance of using these techniques for interpretation of bio-geo-chemical data. After all, for such data the rate of vertical exchange is of imminent importance. All calculations can be performed with observations using the presently most common oceanographic instrument, the CTD and more precisely the SBE911 CTD, and its present post-processing software.

2. Materials and methods

The R/V Pelagia CTD/Rosette system contains a Seabird 911-*plus* Conductivity Temperature Depth system, with the T and C sensors in a duct pumped at a flow rate of 0.027 L s^{-1}. The CTD samples at a rate of 24 Hz. The CTD/Rosette package is lowered via the mid-ship A-frame, which contains a package of springs that ensures some surface-wave-compensation down to about 2000 m. The typical lowering speed averages 0.9 m s^{-1}, typical hoisting speed 0.8 m s^{-1}, so that measurements are made about every 0.04 m. As was noted by Thorpe (1977), this relatively slow descent and ascent rates imply a rather oblique traverse of potentially true and false turbulent overturns, as these can grow over 100 m high in the open ocean (e.g., Klymak et al., 2008). The advantage of such slow rates is that one can reasonably average data in vertical bins < 1 m. Normally, raw CTD-data are averaged into 1–2 m vertical bins, but this yields too coarse displacement-data profiles in our opinion. So, importantly, we here use a smaller vertical-bin-scale of 0.33 m, thereby averaging some 8 data points, and which turns out to be useful for determining overturn shapes. This associates with the typical overturn-scale of 0.4 m found resolvable using CTD-data by Stansfield et al. (2001).

During post-processing, potential surface-wave-influences, that may reverse direction of motion of the package, are filtered out by restricting data to a CTD-speed of >|0.25| m s^{-1}, whereby direction changes are removed. Further post-processing using 2011-SBE-software involved corrections for thermal inertia of conductivity cells. Inspection of the data of notably potential mismatch between the two differently sampled sensors resulted in a slight change in the standard imposed variation in alignment (by +0.033 s instead of 0.073 s advance of the C- with respect to the T-sensor). Nevertheless, the resulting density data are quite noisier, by up to a factor of 10, compared with density inferred from temperature-only data, especially across so-called steps (layers of strong stratification). This confirms earlier findings (by, e.g., Ferron et al., 1998). It is thus advantageous to use temperature-only data, under the condition of a tight T–S relationship.

Temperature sensor data are first transferred to potential temperature (θ) values, before they are used as an estimate for (variations in) potential-density-anomaly $\delta\rho$. Turbulent kinetic energy dissipation rate ε and vertical turbulent eddy diffusivity K_z are estimated by calculating 'overturning' scales using $\alpha\delta\theta$-data, 'temperature-only data', or $\delta\rho$-data. The α denotes the apparent thermal expansion coefficient under local conditions, and which may include contributions from salinity. It is established after fitting a linear power-law to $\delta\rho-\delta\theta$. The overturning scales are obtained after reordering the potential density (temperature) profile, which may contain inversions, into a stable monotonic profile without inversions (Thorpe, 1977,1987). After comparing raw and reordered profiles, displacements (d) are calculated that are necessary for generating the stable profile. In the present paper, the displacements are assigned to the end-point depths, thereby answering the question 'where does the reordered parcel come from'. These 'source-displacements' are thus not assigned to the source-file-depths as in Thorpe (1977). A certain threshold applies to disregard apparent displacements associated with instrumental noise (Ferron et al., 1998). Sophisticated test-methods involve run-length statistics and local T–S relationship criteria (Galbraith and Kelley, 1996) and, specifically for density profiles, (a)symmetric distribution of positive and negative displacements to rule out spikes (Gargett and Garner, 2008). For the 0.33 m binned data this is nominally $<5 \times 10^{-4}$ °C for temperature-data and $<5 \times 10^{-4}$ kg m^{-3} for density data. However, our tests below show that the latter nominal value is too low and should be doubled. Then we estimate

$$\varepsilon = 0.64 d^2 N^3, \tag{1}$$

where N denotes the buoyancy frequency computed from the reordered profile and the constant follows from empirically relating the overturning scale with the Ozmidov scale $L_O = 0.8d$ (Dillon, 1982). Using $K_z = \Gamma \varepsilon N^{-2}$ and a mixing efficiency for the conversion of kinetic into potential energy of $\Gamma = 0.2$ (Osborn, 1980; Oakey, 1982; Ferron et al., 1998; Stansfield et al., 2001), we find

$$K_z = 0.128 d^2 N. \tag{2}$$

For the individual 0.33 m bin scales and an average $\alpha \approx -0.1$ kg m^{-3} °C^{-1} for the present data, the turbulence parameter estimates for temperature-only will be limited to $\varepsilon > 4 \times 10^{-11}$ W kg^{-1}, $K_z > 1 \times 10^{-5}$ m^2 s^{-1} (and $N > 1 \times 10^{-3}$ s^{-1}). These thresholds are valid for most of the ocean, including its weakly turbulent interior, and a fortiori for the main pycnocline that is characterized by values of 2–3 times higher (Gregg, 1989; Polzin et al., 1996). Ideally, one would average (1) and (2) precisely over an overturn (Thorpe, 1977,1987), but as overturns can occur within larger ones, we prefer averaging over a particular vertical range of observations exceeding that of the largest overturns. In the following, averaging over time is denoted by [...], averaging over depth-range by <...>. The specific averaging periods and ranges are indicated with the mean values.

We principally investigate sites where also large internal-wave-induced overturning can be expected, specifically over sub-surface topography. Arbitrarily, two areas are selected, one next to a subsurface ridge of Rockall Bank, West of Ireland, NE Atlantic Ocean (55.5° N, 15.7° W, 960 m water depth), the other halfway the large guyot Mount Josephine, West of Portugal, NE Atlantic Ocean (37° N, 13° W, 2700 m water depth). For reference, we investigate open ocean CTD-profiles from the Canary Basin (30° N, 23° W, 5130 m water depth) around the depth of Mediterranean outflow (800–1400 m).

3. Overturn shapes

Inversions in a density profile are unstable configurations that are dynamically interpreted as overturns induced by turbulent vortical motions. These inversions eventually break and lead to patches of homogeneous density. We investigate the resulting vertical displacement profiles for different idealized overturns, and compare these to observations in the ocean.

3.1. Overturning models

3.1.1. Solid-body-rotation

A purely mechanical overturn of solid-body-rotation forms a z-shape in a stable linear density-depth profile (Fig. 1). Without noise, this single overturn consists of displacements that all lie on the slope ½ in a d–z plane. Such an overturn would preserve mass. However, it is not often observed in reality.

3.1.2. The Rankine vortex

The Rankine vortex (Rankine, 1858) is a more sophisticated 2D-model of a rotating eddy (vortex) in a viscous fluid. It has a particular shape of current, so that at some distance from its center (the 'inner' forced vortex part) as well as at some distance from its edges (the 'outer' free vortex part) the current speed is maximal. Presently, it is a popular model in the x–y plane for atmospheric disturbances like

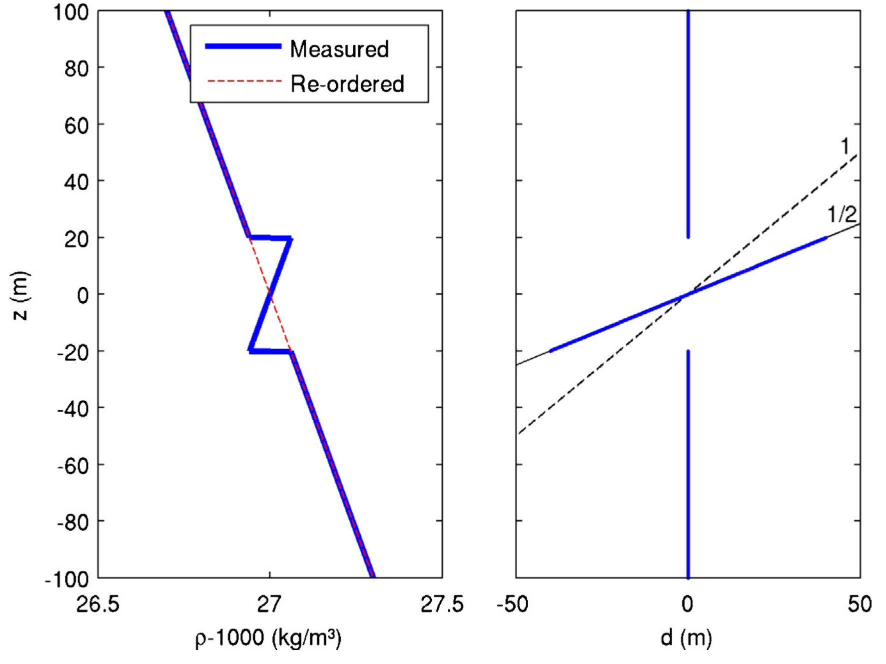

Fig. 1. (left panel) Artificial linear stable density profile over a range of 200 m vertically, with a 40 m thick z-shape profile of instability (blue graph). This profile models a solid-body overturn. The thin red dashed line indicates the same density profile, but after reordering the unstable data points. (right panel) The blue points indicate vertical displacements necessary for reordering the blue profile in the left panel. The solid and dashed black lines indicate slopes in the d–z plane equal to ½ and 1, respectively. (For interpretation of the references to color in the text, the reader is referred to the web version of the article.)

tornadoes. Here it is used in the x–z plane. For its tangential velocity u_θ, of flow V_Γ and radius R, one finds

$$u_\theta = \begin{array}{ll} \dfrac{V_\Gamma r}{2\pi R^2} & \text{for } r < R \\ \dfrac{V_\Gamma}{2\pi r} & \text{for } r > R. \end{array} \tag{3}$$

The result is fluid being varyingly dragged along by the vortex, depending on the distance from its center. This characteristic jet-like structure is significantly different from solid-body-rotation.

We use a simple kinematic model to see how a Rankine vortex modifies density in a stable linearly stratified fluid. After integrating the Rankine motion over half a turn, this kinematic overturn shows a density field, originally linearly increasing with depth, being disturbed like in Fig. 2. The associated displacements shape like Fig. 3, which are characterized by: (a) borders strictly along a slope just exceeding 1 in a d–z plane and which are formed by the upper and lower parts of the density overturn portion (i.e., the parts generated primarily by the free, outer, vortex part), and (b) a slope ranging between ½ and 1 primarily for the forced, inner, vortex part, and mainly denoting the mechanical overturn. Thus, the Rankine vortex introduces two slopes, one which more or less aligns with the long axis of the parallelogram of the solid-body vortex (Fig. 1), and the other which aligns with the maximum displacements possible in an overturn and delineating the sloping parallelogram sides as in Section 3.1.3.

The Rankine-vortex-shape of instability in the otherwise stable density profile (Fig. 3) resembles somewhat the sinusoidal shape-characterization of instabilities that was given by Thorpe (1977) without further explanation. It is noted that the half-turn Rankine vortex does not include overturns at

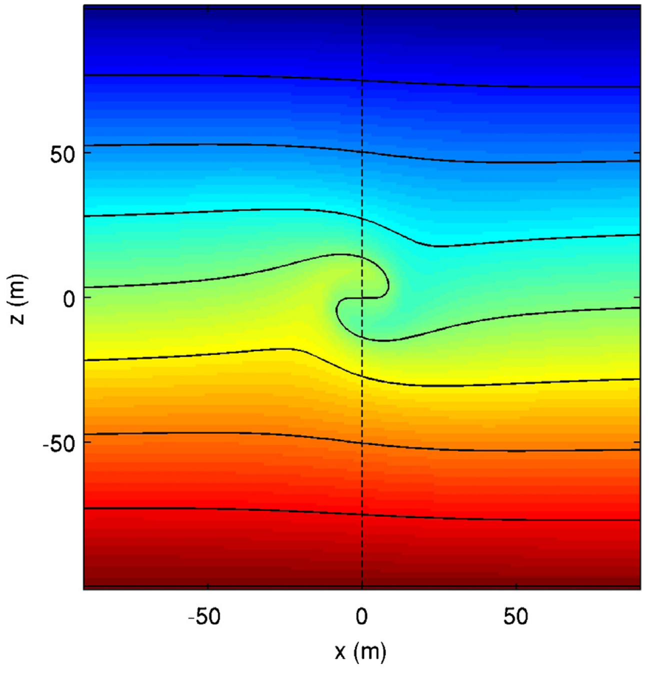

Fig. 2. A stable density stratified basin is overturned by a single half-turn Rankine vortex in its center. This vortex models a 2D-overturn in a viscous fluid. The rather arbitrary colors range from 26.7 to 27.3 kg m^{-3} (dark-blue to deep-red). (For interpretation of the references to color in the text, the reader is referred to the web version of the article.)

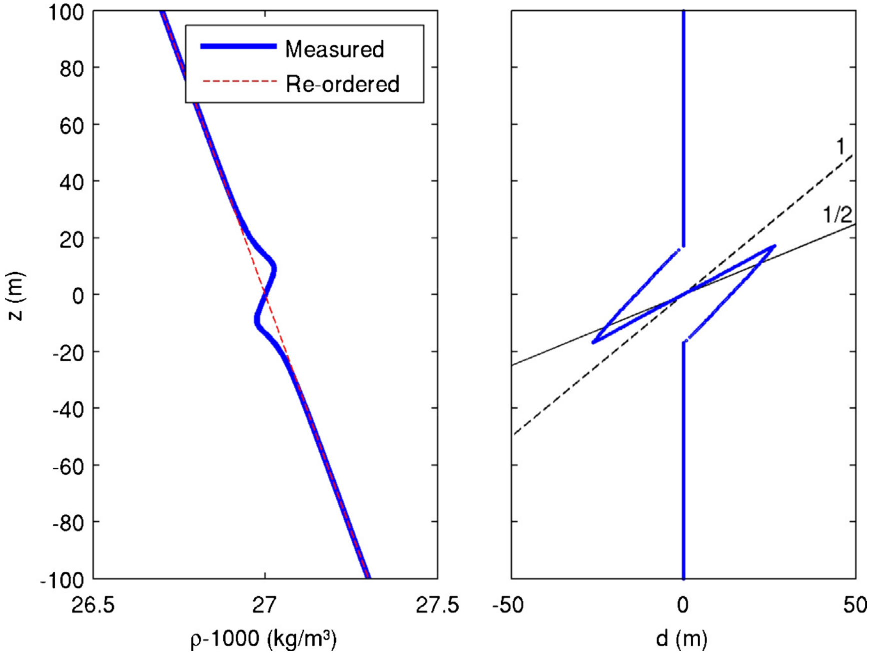

Fig. 3. As Fig. 1, but for the half Rankine vortex in Fig. 2 (along its central dashed line).

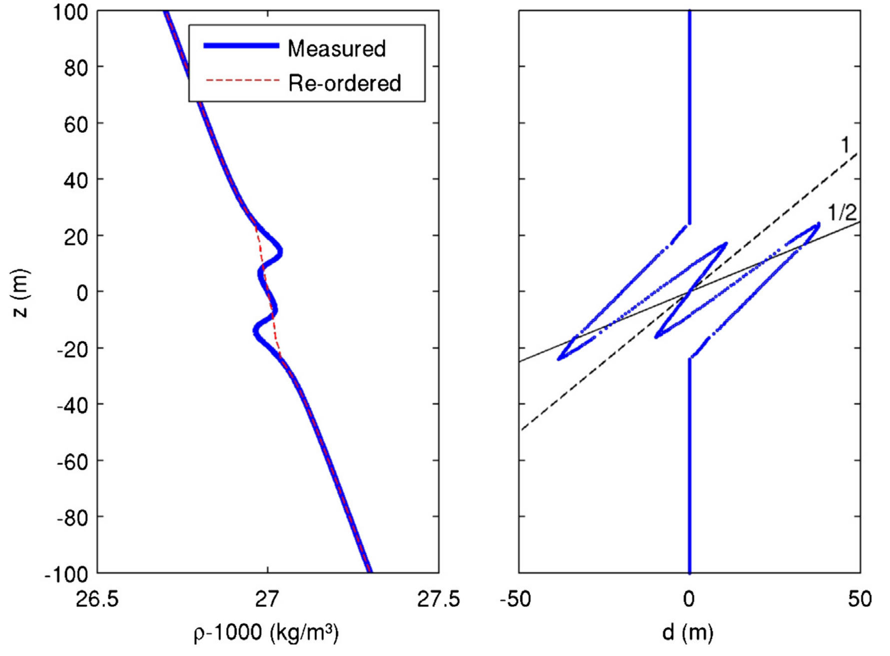

Fig. 4. As Fig. 1, but for a full-turn Rankine vortex.

smaller scales that were suggested by Galbraith and Kelley (1996) to explain the lack of z-shapes in ocean density profiles.

Further integration of the Rankine motion creates smaller vortices in the large one, which result in a split of the overturning slope into slopes that are further away from ½ (but still <1) and away from 1 (the inner core), see Fig. 4 for one full turn. In the case such a split is not observed in ocean density profiles, we suspect that overturns like the Rankine vortex become gravitationally unstable at the point when they reach a half turn. Thereby, they release their potential energy and collapse into smaller turbulent scales and into heat. If so, this implies inertial-buoyancy balance and an overturning time scale $\sim N^{-1}$ for the largest overturns.

3.1.3. *White noise*

A purely homogeneous mixed layer, in fact the result of a complete and irreversible mixing event, will not be reorderable as displacements to their nearest statically stable position are not defined. With some white noise added however, one computes vertical displacements that fill a parallelogram in the d–z plane (Fig. 5). The displacements are limited by the height of the homogeneous layer in an otherwise stable linear density-depth profile resulting in sloping sides of the parallelogram exactly equal to 1 in a d–z plane. The sloping sides denote the maximum displacements that any point of noise can reach following reordering within the near-homogeneous layer. The long-axis of the parallelogram lies on a slope ½ in a d–z plane, which is precisely the theoretical shape of a solid-body overturn.

3.1.4. *Salinity compensated intrusions with diffusion*

The above models are also applicable for temperature data, if temperature can be used as a tracer for density variations, following a tight linear relationship between the two (see Section 4.1.2). In the ocean however, temperature-induced density variations may be perfectly compensated by salinity variations. In that case, overturns that seem apparent in temperature-only profiles are not observed in density (temperature and salinity) profiles. Such temperature-only computations will provide false turbulence estimates. In order to distinguish false displacements we have two tests, (i) the particular

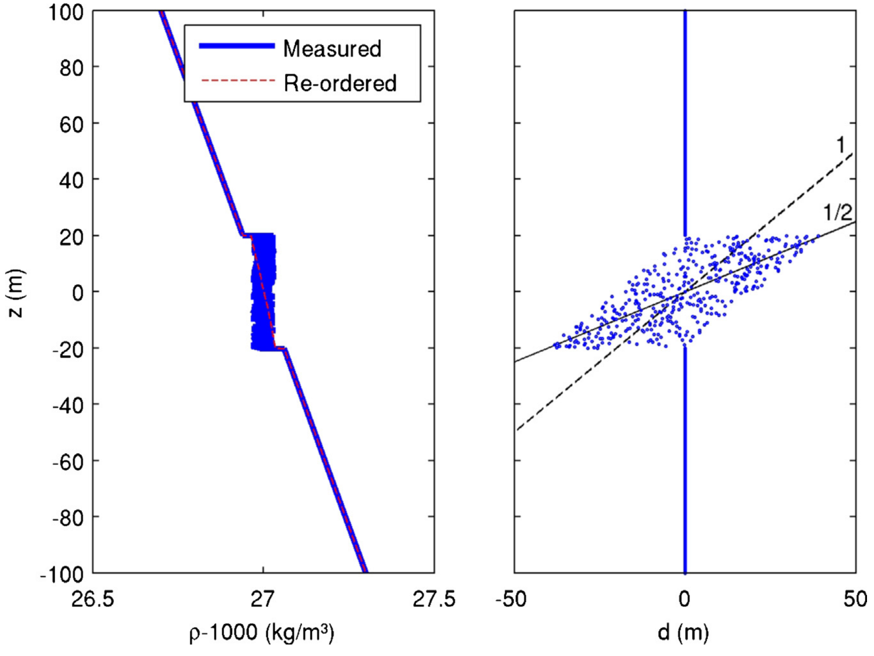

Fig. 5. As Fig. 1, but for a 40 m thick homogeneous layer to which some random noise is added.

shape of 'overturn' to be described here, (ii) the persistence with time of 'overturn' with respect to the buoyancy period. This demands repeated ('yoyo'-profile) or moored observations.

Although the rudimentary shape of a salinity-compensated intrusion of warm-salty water penetrating colder-fresher water of virtually the same density is a block-shaped 'S' as the form in the profile, we will rather consider a (slightly) oblique S-shape to start with (Fig. 6). The former is very unlikely to exist in nature, as sketched in Section 3.1.3. Such an oblique S-shape is characterized by a slow transition above a very fast (sharp) transition in its center. It can be found e.g. following lateral diffusion from a heated wall or a front (Kranenborg and Dijkstra, 1998).

When diffusion/convection is incorporated, especially in the intrusive layer with warm-salty water overlying cooler-fresher water mimicking double-diffusion, the slow transition will be smoothed, but the sharp one barely, see the numerical model results by Walsh and Ruddick (1998). The resulting displacement-shape, whether or not deformed by diffusion, heavily favors a slope of 1 or greater in a d–z plane, even for the long axis of the parallelogram (Fig. 6). It thus distinguishes from the 1D-solid-body and the 2D-Rankine vortex in the previous sub-sections.

3.2. Overturn-displacement observations in the ocean

In this section only downcast temperature profiles are considered from ship-borne CTD. The temperature sensor is the least noisy of the standard CTD-sensors. Comparison with density (salinity/conductivity sensor) data and a comparison between up- and downcast profiles will be discussed in Section 4.

3.2.1. Strong turbulence above Rockall Bank (NE Atlantic)

The lower half of a 950 m long CTD-temperature profile next to a sub-surface topographic ridge in the Rockall Bank area (West of Ireland, NE Atlantic) shows multiple overturns (Fig. 7). In this and subsequent figures the graph including displacements has a grid with the same +1 and +1/2 slopes as

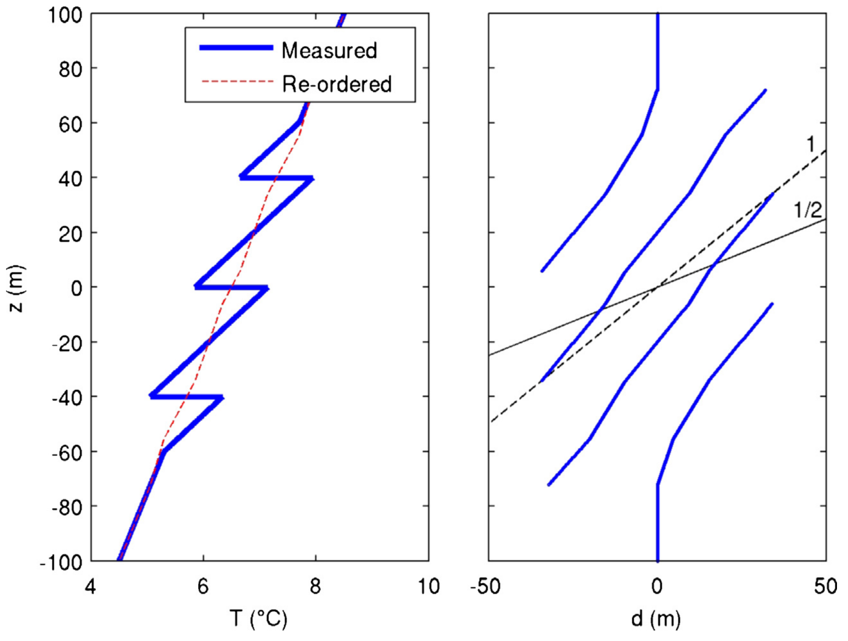

Fig. 6. As Fig. 1, but for a double set of salinity compensated intrusions in a temperature profile, with active convection in the intrusive layers with relatively warmer (saltier) water overlying relatively cooler (fresher) water and no (or weak) diffusion for the transition between cooler over warmer.

in the model figures of Section 3.1. It is noted that we plot displacements as points (Fig. 7b and further) and not like lines (Fig. 7c). Using points, one has a better look inside an overturn.

The temperature inversions related to overturns far exceed the instrumental noise level, which is about 0.0005 °C for 0.33 m scales and after post-processing, and pass the false-overturn tests. The area is thus quite turbulent, not only with multiple overturns, but also with relatively strongly stratified layers in between.

The single profile already shows multiple types of overturns, as inferred from the shape and slopes of the displacements after reordering. (In this case, the direction of reordering is such that stable stratification requires lower (temperature) values below higher ones). From the top down, we see some small overturns between $-550 < z < -500$ m, which seem noise-related, but which are in fact small overturns mainly resembling half-turn Rankine vortices, see the details of slopes of Fig. 3. Between $-670 < z < -570$ m a very large overturn is observed with multiple small ones inside. This system appears slightly erratic, but best resembles a full- (or slightly more) turn Rankine vortex, with near-one (z/d) slopes inside the smaller overturns. In the 50 m further below, between $-730 < z < -670$ m, two medium-size sample half-turn Rankine-displacement shapes can be observed, with each overturn-core having a slope of about halfway between ½ and 1, and the edges just larger than one. Between $-845 < z < -810$ m, we observe two small solid-body-rotation overturns, above multiple small-scale half-turn Rankine vortices. The profile ends some 10 m above the bottom, and well above it several medium-large half-turn Rankine vortices are observed.

The given example is typical for the profiles we observed in this area of Rockall Bank, with a dominance of medium-size half-turn Rankine vortices, an occasional large full-turn Rankine vortex, usually no more than one in a profile, and rarely a, small, solid-body overturn, confirming the remark by Galbraith and Kelley (1996).

3.2.2. Moderate turbulence above a deep seamount slope

As an arbitrary different example, we present a profile of the lower 700 m above mid-depth slope of large underwater guyot Mount Josephine some 220 miles off the coast of Portugal in the NE Atlantic

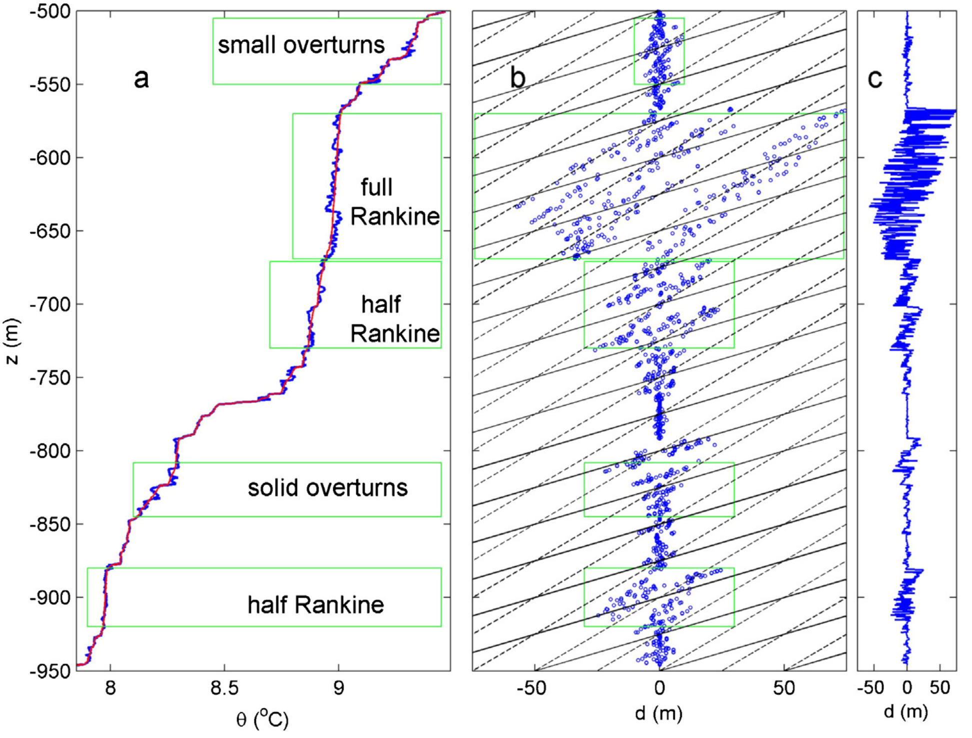

Fig. 7. (a) Example of 450 m, the near-bottom half, of downcast raw potential temperature profile (blue) observed above Rockall Bank. In red its reordered profile. Indicated are some explanations of overturns (see text). (b) Associated displacements (blue dots) in a grid of ½ (solid) and 1 (dashed) slopes in the z/d plane, as in Fig. 1 – right panel. (c) As b, but for the classic way of plotting overturns. (For interpretation of the references to color in the text, the reader is referred to the web version of the article.)

Ocean (Fig. 8). There, around 2500 m, variations in temperature are slightly smaller than above Rockall Bank, stratification is 2.5–3 times weaker (mainly due to a different contribution of salinity) and turbulence is less vigorous. However, the displacements are basically the same, with most of them resembling half-turn Rankine vortices, and very few solid-body overturns and full-turn Rankine vortices. In contrast with the Rockall Bank data, some noise-box filling (cf., Fig. 5) is found in these data, but never to full extent. Noisy data are more found in density profiles.

4. Some particular CTD-observations related to overturns

4.1. Temperature and density

4.1.1. Displacements from density observations

Compared with the temperature data in Fig. 7a, the half-profile of density (including the effects of both temperature and salinity) between −950 and −500 m looks much noisier (Fig. 9a). A few spikes do occur, but otherwise the noise is distributed over the entire profile and not just at the depths of temperature steps. The relatively large noise is found in spite of careful tuning of the two different sensors with different response times by a 3000 rpm pump on the SBE19, and a re-adjustment of the lag-alignment of the sensors during post-processing using the SBE-software. Nonetheless, the displacements (panels b in the above figures) look very similar for the larger overturns, again with a dominance of half-turn Rankine vortices. The large full-turn Rankine vortex seems more symmetric in the density-inferred displacements, although this may be attributed to noise-effects. Only for

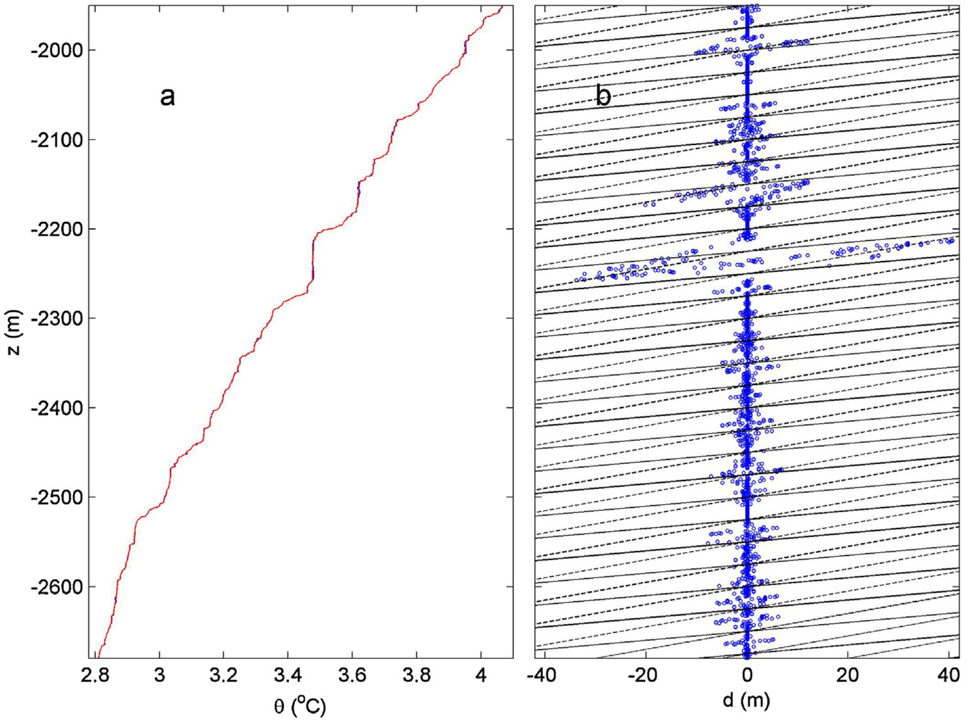

Fig. 8. As Fig. 7(a) and (b), but for the bottom 730 m of a raw density profile above mid-slope of Mount Josephine. Note the different scales.

small overturns some noise-box filling occurs and, with difficulty, evidence of the solid-body overturn around $z = -820$ m is retrieved. For these data, the eventually calculated turbulence parameters differ by less than a factor of 2 compared with those estimated from temperature alone, because the density-temperature relationship is tight.

4.1.2. A tight density-temperature relationship

In order to be able to compare temperature-only inferred displacement data with those estimated from density, the former have to be related linearly via a ‘tight’ relationship to density variations. As seen in Fig. 10a, the 450 m depth-range portion under investigation shows this to be generally the case, at least on the large scale exceeding that of overturns. Here, $\delta\rho = \alpha\delta\theta$, slope $\alpha = -0.136 \pm 0.005$ kg m^{-3} $^\circ$C^{-1} from a linear fit to the data (black dots) and potential temperature can be used as a tracer for density variations. The goodness of fit results in an rms-error of observed – best-fit density variations (Fig. 10b) equal to 0.0018 kg m^{-3}. As a test, the buoyancy frequency determined from reordered temperature-only and density profiles should be equal, using the above relationship. Also, in true turbulent overturns, the turbulence parameter estimates will be near-equal, provided the contribution of noise is limited. Such a tight relationship is regularly found in the ocean, but, as we will see below, not always or everywhere.

4.1.3. Less- and non-tight density-temperature relationships

Above 500 m in the Rockall Bank data, temperature no longer corresponds linearly with density variations due to salinity compensations, presumably following intrusions along isopycnal surfaces or less intense mixing (Fig. 11). Between $-500 < z < 0$ m, displacements that are clearly visible in the temperature-only data are not as clearly found in density-data. The temperature-only displacements are thus partially false overturns, but the relative contributions from intrusions and true overturning

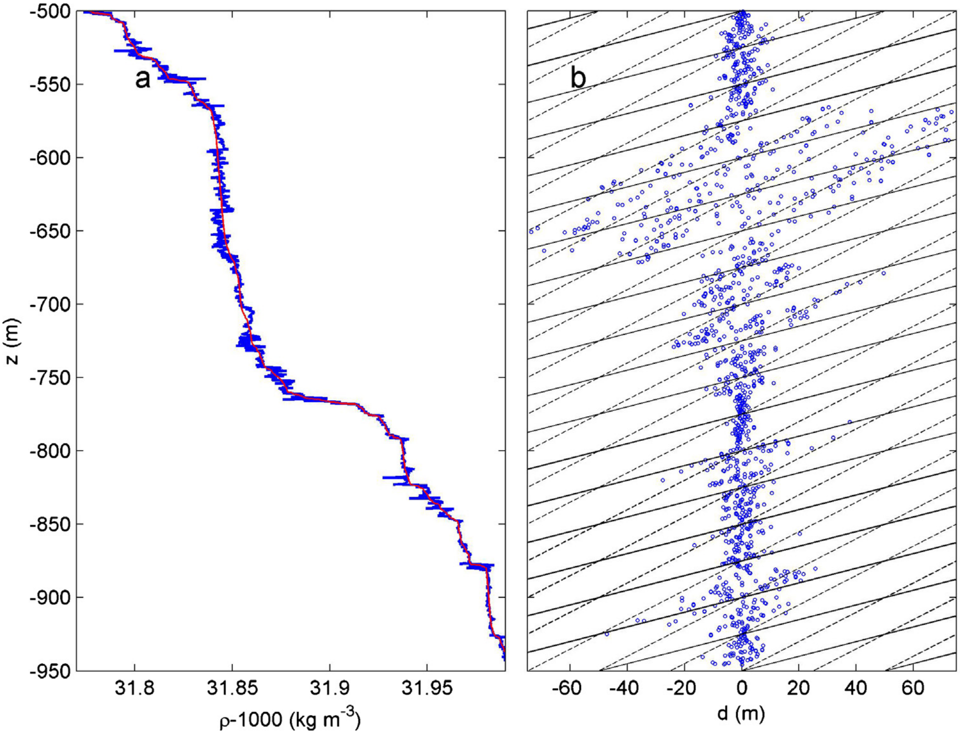

Fig. 9. As Fig. 7(a) and (b) with identical (density, overturn) x–y axes ranges, but for raw downcast density profile.

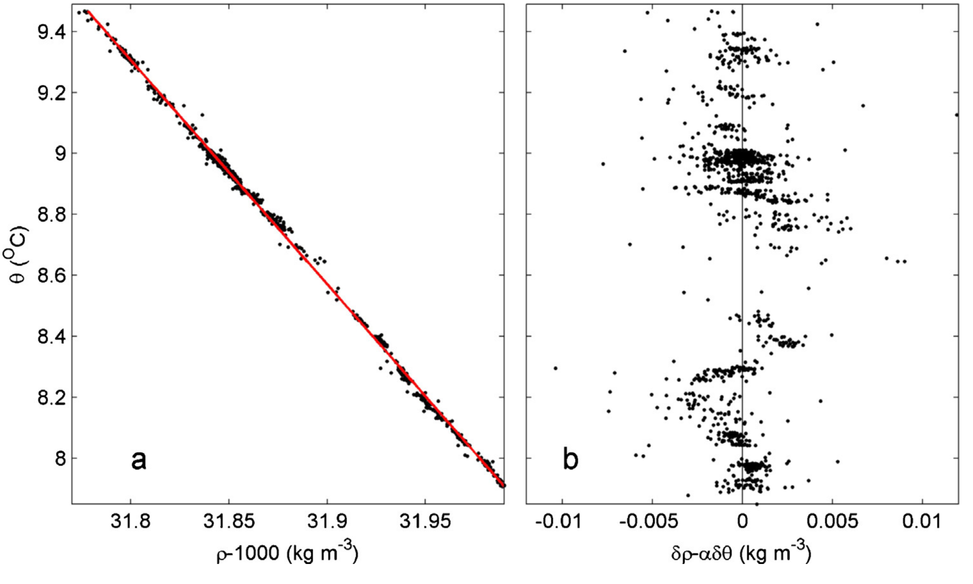

Fig. 10. (a) Density-potential temperature data from Figs. 9 and 7, respectively. In red, their linear relationship is established after a best-fit to the data. (b) The difference between observed density anomaly and linear best-fit estimate from potential temperature data. (For interpretation of the references to color in the text, the reader is referred to the web version of the article.)

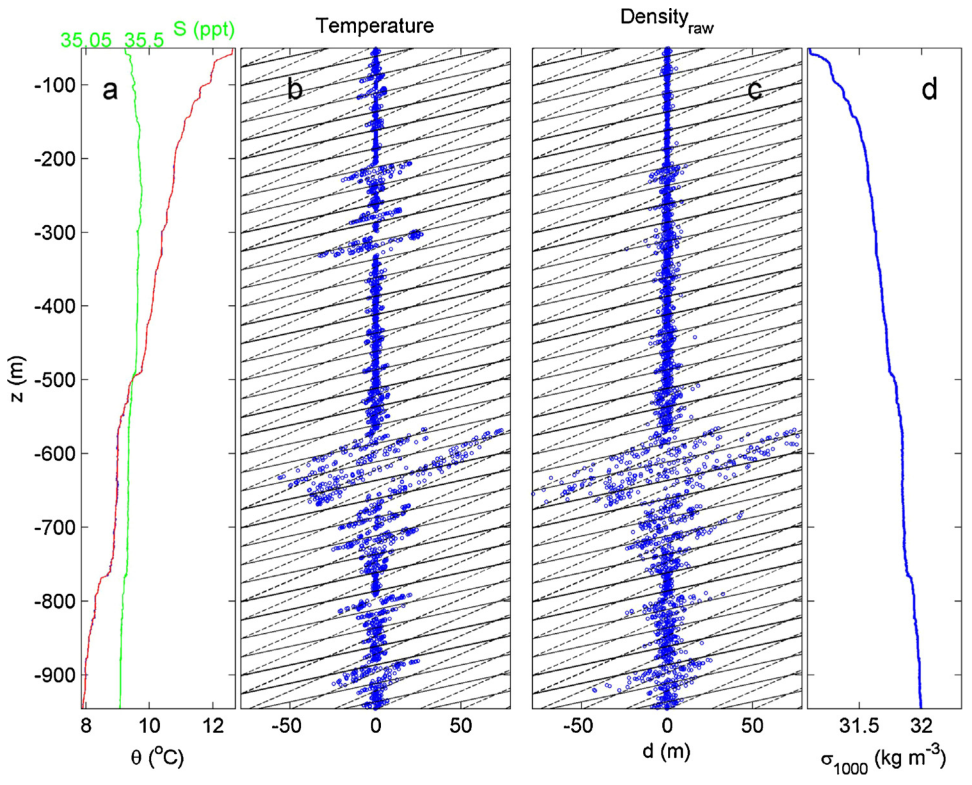

Fig. 11. Comparison of displacement data from Figs. 7b and 9b, but for the nearly full (900 m range) profile. In panel a, salinity is added in green. (For interpretation of the references to color in the text, the reader is referred to the web version of the article.)

are somewhat ambiguous, as the density-data still show some overturning. This may have to do with the near-homogeneity of the layers in which salinity compensation is found (Fig. 11d).

It is noted that in the case of the observational site above Rockall Bank, data shallower than 500 m are far away from bottom topography, whilst those deeper than 500 m are influenced by sloping topography and associated vigorous mixing.

One of the most well-known areas of dominant salinity compensation through intrusions is the Mediterranean outflow into the NE Atlantic Ocean. Mediterranean waters are relatively warm and salty compared to those of the NE Atlantic Ocean. As a result, these waters interleave at their near-equal density levels, causing a sequence of layers of alternating warmer and cooler waters between about 800 and 1400 m, see the example-CTD-profile from the Canary Basin in Fig. 12. It is clearly seen in these data that displacements calculated from a density profile are virtually absent. Note that the layers of salinity compensation are still stratified in density (Fig. 12d), which contrasts with such layers found in the upper part of Rockall Bank area (Fig. 11d). Displacements calculated from temperature-only are very large, and show a much steeper slope than those from the Rockall Bank. The long axis of the parallelogram deviates strongly from ½ (z/d), often being very close to 1 (z/d), as predicted by the model of Section 3.1.4 for typical intrusion-like temperature profiles. However, exceptions to the rule do occur, e.g., the small apparent-overturn around 1330 m. This requires more complex modeling of intrusions or an additional test for separating real from false overturns.

A CTD-test of persistence with time can be made by repeated lowering and hoisting in a 'yoyo'-fashion (e.g., Alford and Pinkel, 2000). This should be maintained for at least several buoyancy periods. Inversions that vanish over a period shorter than the buoyancy period are likely due to turbulent overturns (e.g., Riley et al., 1981). Inversions longer persistent than the buoyancy period are likely

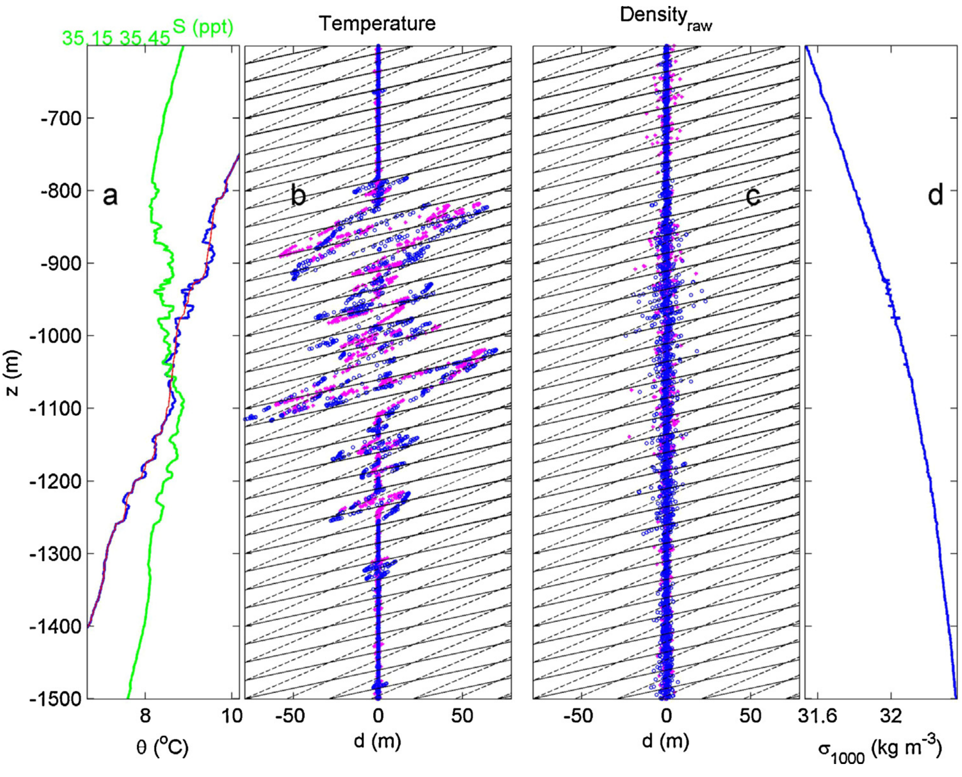

Fig. 12. As Fig. 11, but for open Canary Basin (30° N, 23° W, 5130 m water depth) CTD-profile around the depth of Mediterranean outflow waters. In (b) and (c), the purple symbols indicate displacements calculated for the upcast profile.

to be the signature of internal wave motions (Groen, 1948) or, in this case, salinity compensated intrusions. Of course, this is not an exclusive test, as larger-scale motions may advect shorter-scale overturns beyond the location where CTD-yoyo profiles are made. It should thus be used in conjunction with the above displacement-shape test.

A natural yoyo-profile is obtained by the down- and upcast-data in a single CTD-profile (noting the potential problems of smoothing by the Rosette frame given below). The deep-ocean temperature profile of Fig. 12 takes another 7500 s to return to 1400 m from its journey to the bottom (5130 m) and back. Here and elsewhere, the ship did not move more than half its length horizontally during the duration of overboard operation. However, the local buoyancy period is 2150 s, so that any displacement observed during downcast and remaining visible around the same depth in the upcast profile may, very likely, be attributable to a false overturn. It is seen that the displacements between 1000 and 1400 m all, including the one around 1330 m, are visible in the purple (upcast) profile. They are thus false overturns.

4.2. Down- and upcasts

4.2.1. Mechanical smoothing during upcast

So far we were mainly concerned with downcast profiles, during which the CTD-instrument package is principally lowered. As the CTD-sensors are located near the bottom-center of the about 2 m^3 large Rosette-frame holding water bottles besides electronic sensors, it is thus considered that the system is traversing and sampling mostly undisturbed waters. However, during an upcast the bulk of the Rosette-frame is passing through and disturbing water-properties before they reach the

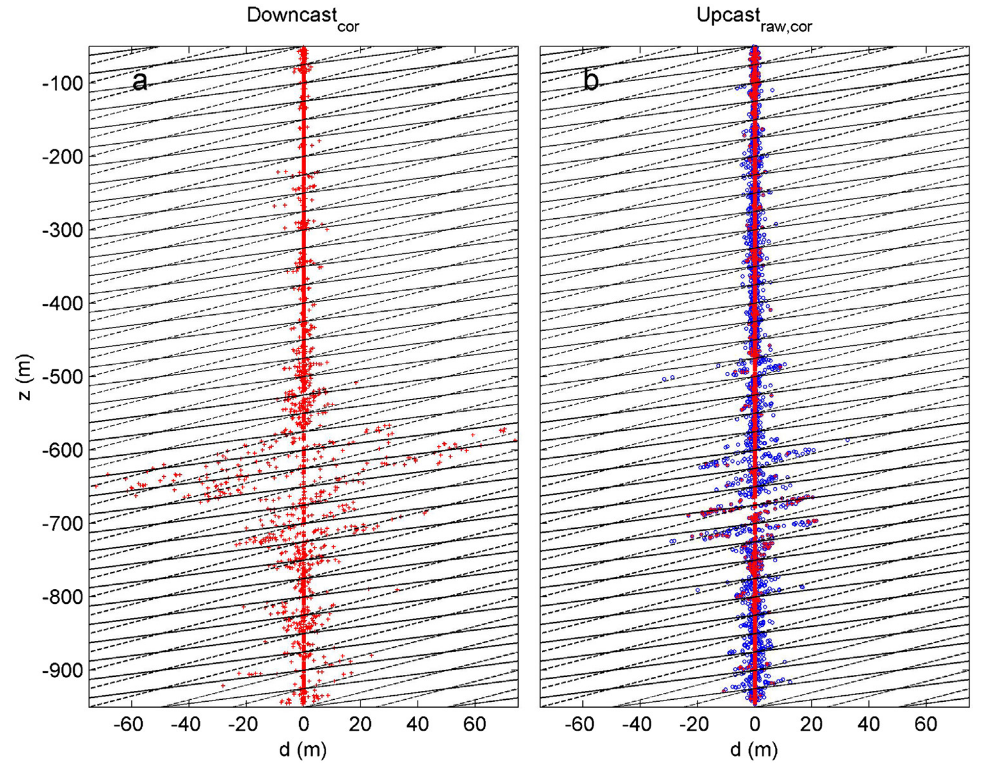

Fig. 13. (a) As Fig. 11b, but for displacements computed from corrected data after removal of density variations smaller than 10^{-3} kg m^{-3}, twice the expected noise level. (b) As panel (a), but for upcast density data, raw data (blue) and noise-corrected data (red). (For interpretation of the references to color in the text, the reader is referred to the web version of the article.)

CTD-sensors. This is commonly known to oceanographers, but here we demonstrate how different upcast-data can be from downcast-data in terms of overturning properties.

Fig. 13 shows that the upcast (Rockall Bank) density data are, in appearance, less noisy than the downcast data obtained immediately before (the CTD is stopped less than 10 s at its deepest point). When corrected for sensor mismatch and other instrumental post-processing, and after discarding all density variations smaller than 10^{-3} kg m^{-3}, twice the expected instrumental noise level of 5×10^{-4} kg m^{-3} (resulting in corrected red-crosses), the upcast-data are almost as noiseless as temperature-only data. The noise-reduction causes the larger overturn displacements to be as clearly visible as in temperature data; in the upcast-data they are also clearly dominated by half-turn Rankine vortices. However, the effect of the upcast, i.e., the bulkhead of Rosette-frame and the tail-positioning of the CTD-sensors, also has a dramatic reducing effect on the evaluation of large displacements. In particular, the full-turn Rankine vortex is reduced in size. Such overturns are generally found in layers of weak stratification. The maximum displacement is reduced by a factor of 2 with respect to that of the downcast, which causes a reduction by a factor of 4 for turbulence parameters. The layers of largest overturns between $-750 < z < -600$ m are not displaced much vertically in the 10 min between the two passages.

The above observations are not unique, but are found in nearly all profiles of both sets of data presented here. Not only are the turbulence parameters different by, on average, a factor of 4 when computed from density down- and upcast profiles, but also when they are computed from temperature-only down- and upcast profiles. This generality is shown below for Mount Josephine data.

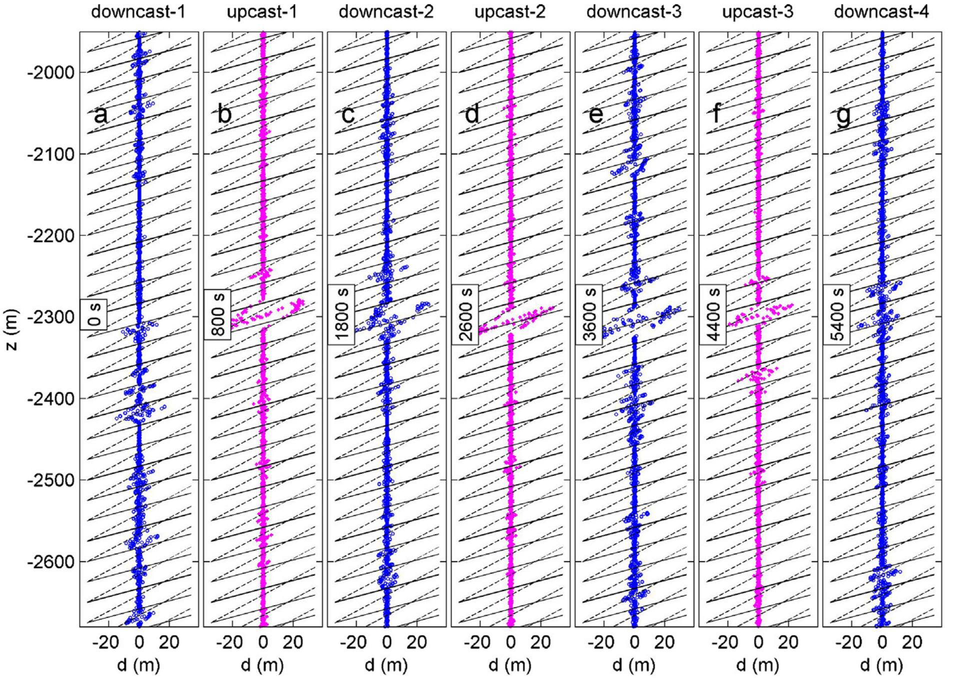

Fig. 14. As Fig. 13, but for displacements computed for a repeated three-and-a-half set of 700-m-range subsequent down- and upcast temperature profiles above Mount Josephine.

4.2.2. *Persistence of overturns*

In Fig. 14, three-and-a-half repeat down- and upcast profile pairs of temperature displacements are shown (out of 21 from a 700 m vertical yoyo-range above Mount Josephine). As before, during the entire operation the ship was actively held on position and drifted less than 30 m horizontally. The observations are thus essentially Eulerian. The above-mentioned reduced 'noise' is seen in most upcast profiles, compared with the downcast profiles. In this example, the larger overturns are less affected than in the Rockall Bank data of Fig. 13. Nonetheless in these data too, the turbulence parameters averaged over the entire vertical range of 700 m are reduced by a factor of 3–5 for the upcasts. This is partially due to the missing small-scale overturns in the upcast and to the reduced number of large overturns and, less so in the presented example, in their reduced size. Otherwise, the shapes of the overturns remain all similar: a dominance of half-turn Rankine vortices.

As the average time between mid-range (∼2300 m) passages is about 900 s, and as most small overturns cannot be clearly traced between passages at such an interval of time, it seems that we are indeed observing 'true' overturns as sketched in Section 3.1. The one large overturn near 2300 m lasts from upcast-1 to upcast-3, with a clear half-Rankine signature during upcast-2. The total duration is 4400 ± 800 s. This is less than the local buoyancy period of 5700 s, so that even this overturn is expected to represent a turbulent overturn. Potentially false overturns due to salinity-compensated intrusions are not dominating these observations. This is not only concluded following very similar, but noisier, associated density-inferred displacements and because such intrusions generally have a much longer duration. It is also concluded because of the displacement shape, which deforms somewhat over time but always best resembles the Rankine-vortex model-shape.

5. Discussion and conclusions

An additional, more direct and dynamical way of discriminating various overturns and (false overturn-) intrusions in vertical profile observations in the ocean is the here proposed inspection

Table 1
A comparison of turbulence parameter estimates from CTD-observations computed for various locations and different computations. Abbreviation pa = profiles average.

Rockall Bank [−950, −500] m [<N>] = 2.5×10^{-3} s^{-1}	3 pa [<ε>] (W kg^{-1})	3 pa [<K_z>] (m^2 s^{-1})
Downcast θ	1.8×10^{-7}	1.5×10^{-2}
Upcast θ	4.0×10^{-8}	2.5×10^{-3}
Downcast ρ_{raw}	4.0×10^{-7}	2.0×10^{-2}
Downcast ρ_{cor} (>1×10^{-3} kg m^{-3})	2.8×10^{-7}	1.2×10^{-2}
Upcast ρ_{raw}	1.0×10^{-7}	3.8×10^{-3}
Upcast ρ_{cor} (>1×10^{-3} kg m^{-3})	6.0×10^{-8}	1.3×10^{-3}
Rockall Bank [−950, −50] m [<N>] = 3.2×10^{-3} s^{-1}	**3 pa [<ε>] (W kg^{-1})**	**3 pa [<K_z>] (m^2 s^{-1})**
Downcast θ	1.7×10^{-7}	1.1×10^{-2}
Upcast θ	1.2×10^{-7}	6.0×10^{-3}
Downcast ρ_{raw}	1.5×10^{-7}	9.3×10^{-3}
Downcast ρ_{cor} (>1×10^{-3} kg m^{-3})	1.0×10^{-7}	5.2×10^{-3}
Upcast ρ_{raw}	5.0×10^{-8}	2.1×10^{-3}
Upcast ρ_{cor} (>1×10^{-3} kg m^{-3})	2.0×10^{-8}	6.0×10^{-4}
Mnt Josephine [−2680, −1980] m [<N>] = 1.1×10^{-3} s^{-1}	**21 pa [<ε>] (W kg^{-1})**	**21 pa [<K_z>] (m^2 s^{-1})**
Downcast θ	2.1×10^{-9}	5.4×10^{-4}
Upcast θ	4.0×10^{-10}	1.9×10^{-4}
Downcast ρ_{raw}	3.1×10^{-8}	2.1×10^{-3}
Downcast ρ_{cor} (>1×10^{-3} kg m^{-3})	2.3×10^{-9}	1.6×10^{-4}
Upcast ρ_{raw}	1.5×10^{-8}	1.5×10^{-3}
Upcast ρ_{cor} (>1×10^{-3} kg m^{-3})	4.6×10^{-9}	3.6×10^{-4}

of displacement-shapes in a (d, z)-plane. It is found that most true overturns can be modeled as half-turn Rankine vortices, with very few contributions from solid-body-rotations. The slopes in a d–z plane of both the central line of overturn and the entire box, discriminate the Rankine vortex from salinity-compensated intrusions, in most cases. The additional investigation of persistence with time should be sufficient for complete discrimination, especially for high-sampling rate moored thermistor string observations. This results in time-scale-estimates of overturns, the largest approaching N^{-1} (*cf*., Fig. 14).

The most commonly observed half-turn Rankine vortices suggest a dynamical model for vertical overturns in a stratified fluid which bares resemblance to horizontal vortices (in a homogenous or stratified fluid). The half-turn Rankine vortex of Fig. 14 has a time-scale of the order of N^{-1}. This is the upper limit time-scale of overturns, in the sense that buoyancy effects are supposed to become dynamically significant after one buoyancy period. Half-turn Rankine vortices are observed (*cf*., Fig. 7) to have medium vertical extent of several 10's of meters in locally near-homogeneous layers. The rather rare full-turn Rankine vortices are only observed in very large near-homogeneous layers O(100 m). Their duration is well-shorter than N^{-1}. The rare solid-body overturns are all observed small, well-less than 10 m, short-lived and generally in locally rather strong stratification.

Confirming previous validity tests, (Galbraith and Kelley, 1996; Ferron et al., 1998; Stansfield et al., 2001), the present 24-Hz sampled SeaBird 911 CTD-data seem useful for estimating overturn displacements and turbulence parameters, provided they are binned in relatively small scales (here 0.33 m). Best results are obtained using the relatively low-noise temperature-only data. However, this is only dynamically useful in areas where salinity compensated intrusions are negligible. This has always to be verified (using CTD).

In such cases where intrusions are negligible, the increased noise due to the use of two sensors determining density causes an overestimate of turbulence parameters, even for post-processed data from a pumped SBE19 unit. (Temperature-only data are thus giving lower values than density data). More or less equal values, to within a factor of about 1.5, are only obtained by imposing a limit of discarding density variations smaller than twice the estimated standard error (<1×10^{-3} kg m^{-3}; see Table 1). Unfortunately, this limits the use of investigating the shape of displacements from density data in most ocean waters. For these waters and such cases, one can best use temperature-only data that are also applicable in rather strongly stratified, weakly turbulent layers such as the main pycnocline.

The CTD-upcast systematically underestimates turbulence parameters, by a factor of 3–5 compared to downcast profiles. This confirms earlier conclusions by, e.g., Thorpe (1977) that upcast-profile-data are not so useful for estimating turbulence parameters. However, upcast-data are found useful here for investigation of persistence of overturns and/or intrusions with time. Such an investigation can be done using a single set of down- and upcast profiles, but better in a repeated 'yoyo'-set of profiles. If this is done over a limited range of depths, whereby the CTD is left underwater during the entire session of profiles, we note that the first and last 30 s of data are better discarded. In the present data it is found that halting the instrument at a particular depth, for creating a new file, caused such a mismatch between T and S, that bad density data were obtained in the subsequent few 10's of m of up- or downcast immediately thereafter. This may be due to obstruction of the Rosette frame.

The presented turbulence estimates from overturn-displacement-data have not been compared with those estimated from microstructure profiler small-scale shear- or from Lowered Acoustic Doppler Current Profiler large-scale shear data. Such a comparison has been done previously (e.g., Hosegood et al., 2005), with a generally good agreement to within a factor of two. This is similar to results following a comparison between turbulence parameter estimates from CTD-overturn displacements with those from microstructure profiler shear (e.g., Stansfield et al., 2001).

The ubiquity of CTD-observations allows for general turbulence exchange studies, provided the data are obtained using well-calibrated sensors and provided they are available as raw data to allow some fine-tuned post-processing. This can be an important support for a number of marine biology and marine geology studies and which is too little explored so far. To this end, the provided additional information on overturn shape may prove useful.

Acknowledgments

We thank captain and crew of R/V Pelagia for the many pleasant cruises and numerous CTD-profiling. The Rockall Bank data were collected during the 'Corals 2012' cruise of F. Mienis. This paper was mainly written during a one month stay of HvH as a visiting professor at and financed by the École Centrale de Lyon. LG was supported in part by ANR 2011 Blanc SIMI 5-6 012-03 (OLA).

References

Alford, M.H., Pinkel, R., 2000. Observations of overturning in the thermocline: the context of ocean mixing. J. Phys. Oceanogr. 30, 805–832.
Cairns, J.L., Williams, G.O., 1976. Internal wave observations from a midwater float. 2. J. Geophys. Res 81, 1943–1950.
Dillon, T.M., 1982. Vertical overturns: a comparison of Thorpe and Ozmidov length scales. J. Geophys. Res. 87, 9601–9613.
Ferron, B., Mercier, H., Speer, K., Gargett, A., Polzin, A., 1998. Mixing in the Romanche Fracture Zone. J. Phys. Oceanogr. 28, 1929–1945.
Galbraith, P.S., Kelley, D.E., 1996. Identifying overturns in CTD profiles. J. Atmos. Oceanic Technol. 13, 688–702.
Gargett, A., Garner, T., 2008. Determining Thorpe scales from ship-lowered CTD density profiles. J. Atmos. Oceanic Techol. 25, 1657–1670.
Gregg, M.C., 1989. Scaling turbulent dissipation in the thermocline. J. Geophys. Res. 94, 9686–9698.
Groen, P., 1948. Contribution to the theory of internal waves. Koninklijk Nederlands Meteorologisch Instituut, de Bilt, NL. Med. verh. ser. B, 2, vol. 11A, 23 pp.
Hosegood, P., van Haren, H., Veth, C., 2005. Mixing within the interior of the Faeroe-Shetland Channel. J. Mar. Res. 63, 529–561.
Jiménez, J., 1997. Oceanic turbulence at millimeter scale. Sci. Mar. 61 (Suppl. 1), 47–56.
Klymak, J., Pinkel, R., Rainville, L., 2008. Direct breaking of the internal tide near topography: Kaena Ridge. J. Phys. Oceanogr. 38, 380–399.
Kranenborg, E.J., Dijkstra, H.A., 1998. On the evolution of double-diffusive intrusions into a stably stratified liquid: a study of the layer merging process. Int. J. Heat Mass Transfer 41, 2743–2756.
LeBlond, P.H., Mysak, L.A., 1978. Waves in the Ocean. Elsevier, Amsterdam, 602 pp.
Marmorino, G.O., Rosenblum, L.J., Trump, C.L., 1987. Fine-scale temperature variability: the influence of near-inertial waves. J. Geophys. Res. 92, 13049–13062.
Oakey, N.S., 1982. Determination of the rate of dissipation of turbulent energy from simultaneous temperature and velocity shear microstructure measurements. J. Phys. Oceanogr. 12, 256–271.
Osborn, T.R., 1980. Estimates of the local rate of vertical diffusion from dissipation measurements. J. Phys. Oceanogr. 10, 83–89.
Polzin, K.L., Speer, K.G., Toole, J.M., Schmitt, R.W., 1996. Intense mixing of Antarctic Bottom Water in the equatorial Atlantic Ocean. Nature 380, 54–57.
Rankine, W.J.R., 1858. A Manual of Applied Mechanics. R. Griffin & Co., Glasgow, UK, 676 pp.

Riley, J.J., Metcalf, R.W., Weissman, M.A., 1981. Direct numerical simulations of homogeneous turbulence in density-stratified fluids. In: West, B.J. (Ed.), Nonlinear Properties of Internal Waves. Am. Inst. Phys., New York, USA, pp. 79–112.
Shrira, V.I., 1981. On the propagation of a three-dimensional packet of weakly non-linear internal gravity waves. Int. J. Nonlin. Mech. 16, 129–138.
Stansfield, K., Garrett, C., Dewey, R., 2001. The probability distribution of the Thorpe displacement within overturns in Juan de Fuca Strait. J. Phys. Oceanogr. 31, 3421–3434.
Thorpe, S.A., 1977. Turbulence and mixing in a Scottish loch. Phil. Trans. Roy. Soc. Lond. A 286, 125–181.
Thorpe, S.A., 1987. Current and temperature variability on the continental slope. Phil. Trans. Roy. Soc. Lond. A 323, 471–517.
van Haren, H., 2005. Internal waves near the buoyancy frequency in a narrow wave-guide. J. Sea Res. 53, 121–129.
Walsh, D., Ruddick, B., 1998. Nonlinear equilibration of thermohaline intrusions. J. Phys. Oceanogr. 28, 1043–1070.